

Quasinormal modes for charged Lifshitz black holes with scalar hair

Shan Wu^{1*}, Rui-Hong Yue^{1†}, Ming Zhang^{2‡}

and De-Cheng Zou^{3§}

¹*Center for Gravitation and Cosmology, College of Physical Science and Technology,
Yangzhou University, Yangzhou 225009, China*

²*Faculty of Science, Xi'an Aeronautical University, Xi'an 710077 China*

³*College of Physics and Communication Electronics,
Jiangxi Normal University, Nanchang 330022, China*

In this paper, we focus on the generalized Einstein-Maxwell-Dilaton (EMD) gravity, including a nonminimal coupling term between the Maxwell field and scalar field. We construct charged Lifshitz black holes with scalar hair of EMD gravity in the presence of cosmological constant for various horizon topologies ($k = 0, \pm 1$). Then, we consider the scalar perturbations of charged Lifshitz black hole solutions and explore quasinormal modes (QNMs) of these black holes. By using the improved asymptotic iteration method (AIM), we recover the effects of factors such as the curvature, mass, and critical dynamic exponent of black holes on the QNMs.

I. INTRODUCTION

The no-hair theorem[1, 2] is a core principle in black hole physics, stating that the properties of a black hole are uniquely determined by three parameters: mass, charge, and angular momentum. This theorem has been widely supported within the frameworks of Einstein's theory of gravity and Maxwell's electromagnetic theory, as the external field of a black hole in these theories follows Gauss's law, indicating that conserved quantities are closely related to the black hole's characteristics. However, with the introduction of scalar fields and other physical fields[3–6], such as the Einstein-Yang-Mills SU(2) coupled system, black holes with Skyrme hairs and black holes with dilaton hairs, it has been found that the existence of these fields may lead to a violation of the no-hair theorem[7]. Notably, in cases of conformally coupled scalar fields, “hairy black holes” can emerge, which possess additional macroscopic degrees of freedom that make their external field behavior no longer conform to the no-hair theorem. The phenomenon of spontaneous scalariza-

* 18155514717@163.com

† Corresponding author: rhyue@yzu.edu.cn

‡ Corresponding author: mingzhang0807@126.com

§ dczou@jxnu.edu.cn

tion was explored in the context of neutron stars[8], revealing that effective non-minimal coupling between the scalar field and curvature can lead to non-trivial behavior of black holes, potentially resulting in changes to the total mass. This scalarization of black holes may only manifest features under strong gravitational backgrounds, and it could provide new insights into the nature of black hole scalarization with the help of emergent technologies like gravitational wave detectors (such as LISA) and black hole shadow imaging[9]. Recently, Herdeiro *et al.* [10] proposed an Einstein-Maxwell-scalar model characterized by a non-minimal coupling between the scalar field and the Maxwell field. Subsequently, Alfredo and Moreira *et al.* [13–15] have also proposed new exact black hole solutions within the framework of generalized Einstein-Maxwell-Dilaton theory, arising from the breaking of spacetime isotropic scale symmetry. Lifshitz spacetime serves as a natural framework for the gravitational dual of non-Lorentz invariant quantum field theories[16]. In this work, we present the metric for Lifshitz spacetime as follows:

$$ds^2 = -\left(\frac{r}{l}\right)^{2z} dt^2 + \frac{l^2}{r^2} dr^2 + r^2 d^2\Omega. \quad (1)$$

The metric remains invariant under scaling transformations, with the anisotropy of the scaling symmetry quantified by the critical dynamical exponent z

$$t \mapsto \lambda^z t, \quad r \mapsto \lambda^{-1} r, \quad x_i \mapsto \lambda x_i. \quad (2)$$

Gravitational wave detection has made significant advances in astrophysics and the study of black holes, providing a reliable method for investigating black hole oscillations or mergers[17–20]. Modern detectors like LIGO and Virgo effectively capture these signals, and by analyzing the frequency and amplitude in the waveforms, one can infer the mass, spin, and merger process of black holes. This deepens our understanding of black holes and offers new avenues for testing fundamental gravitational theories. Black holes interact with surrounding matter, producing gravitational waves that manifest as brief radiation bursts and damped oscillations, known as quasinormal modes (QNMs). QNMs are crucial for describing dissipative systems and black hole physics, the real part of the complex frequency represents the oscillation frequency, and the imaginary part reflects the decay time scale. Analyzing the QNMs from astrophysical black holes helps in understanding the existence of extra dimensions in string theory[21–23]. In addition, QNMs helps to infer the mass and angular momentum of the black hole and test the no-hair theorem of general relativity[24, 25], providing evidence for echoes in the ring-down signal[26]. QNMs play an important role in assessing the stability of background spacetimes and are key to identifying the existence of black holes and their dynamic stability. This paper will investigate the QNMs of the charged Lifshitz black holes

with scalar hair, exploring the impact of model parameters on the dynamics of perturbation waves and testing the stability of the background configuration.

The organization of this paper is as follows: In Sec. II, we introduce the theoretical framework of higher-dimensional Lifshitz black holes with non-minimal coupling between scalar and Maxwell fields, and discuss scalarized Lifshitz black holes for various horizon topologies ($k = 0, \pm 1$). In Sec. III, we investigate scalar perturbations and use an improved asymptotic iteration method (AIM) to calculate the QNM frequencies of charged higher-dimensional Lifshitz black holes. In Sec. IV, we analyze the numerical results of the QNMs and study the effects of factors such as the curvature, mass, and critical dynamical exponent of the black hole on the QNMs. Finally, we conclude the paper with closing remarks in Sec. V. Throughout the text, we adopt the metric signature $(-, +, +, +)$.

II. SOLUTIONS OF CHARGED LIFSHITZ BLACK HOLES

In this study, we will explore the solutions to a generalized Einstein-Maxwell-Dilaton setup in high-dimensional space. Namely, the action of our framework reads as

$$S = \frac{1}{16\pi} \int d^D x \sqrt{-g} \left[\frac{R - 2\lambda}{2\kappa} - \frac{1}{2} \partial_\mu \phi \partial^\mu \phi - \frac{h(\phi)}{4} F_{\mu\nu} F^{\mu\nu} \right], \quad (3)$$

where $g = \det(g_{\mu\nu})$ denotes the metric determinant, R is the Ricci scalar, κ is the Einstein's gravitational constant, λ is the cosmological constant, $F_{\mu\nu} = \partial_\mu A_\nu - \partial_\nu A_\mu$ is the standard Maxwell field and we recall that $h(\phi)$ is a nonminimal coupling function.

Varying the action (3) with respect to the metric $g_{\mu\nu}$, dilaton field ϕ , and electromagnetic potential A_μ leads to

$$\nabla^2 \phi - \frac{1}{4} \frac{dh}{d\phi} F_{\mu\nu} F^{\mu\nu} = 0; \quad (4)$$

$$G_{\mu\nu} + \lambda g_{\mu\nu} - \kappa T_{\mu\nu} = 0; \quad (5)$$

$$\nabla_\nu (h(\phi) F^{\mu\nu}) = 0, \quad (6)$$

where $G_{\mu\nu} = R_{\mu\nu} - \frac{1}{2} R g_{\mu\nu}$ is the Einstein tensor, $T_{\mu\nu}$ is the energy-momentum tensor:

$$T_{\mu\nu} = \partial_\mu \phi \partial_\nu \phi - \frac{1}{2} g_{\mu\nu} (\partial\phi)^2 + F_{\mu\alpha} F_\nu^\alpha - \frac{1}{4} F_{\alpha\beta}^{\alpha\beta} g_{\mu\nu}. \quad (7)$$

We assume the metric of Lifshitz spacetime taking the following form

$$ds^2 = - \left(\frac{r}{l} \right)^{2z} f(r) dt^2 + \frac{dr^2}{\left(\frac{r}{l} \right)^2 f(r)} + r^2 \sum_{d=1}^{D-2} d^2 \Omega_d, \quad (8)$$

where z is dynamical critical exponent and $d^2\Omega_k$ represents the line element given by

$$d^2\Omega_k = \begin{cases} d\theta_1^2 + \sin^2 \theta_1 (d\theta_2^2 + \sin^2 \theta_2 (+ \dots + \sin^2 \theta_{D-3} d^2\theta_{D-2})) & k = 1; \\ d\theta_1^2 + d\theta_2^2 + \dots d\theta_{D-2}^2 & k = 0; \\ d\theta_1^2 + \sinh^2 \theta_1 (d\theta_2^2 + \sinh^2 \theta_2 (+ \dots + \sinh^2 \theta_{D-3} d^2\theta_{D-2})) & k = -1. \end{cases} \quad (9)$$

Note that the fields to inherit the spacetime isometries such that they are functions of the r coordinate only. The vector potential is taken to be of the purely electrical form, thus, the field ansatzes are:

$$\phi = \phi(r), \quad A = V(r)dt. \quad (10)$$

Substituting the metric ansatz (8) and Eq. (10) into the Maxwell equation (6), we have

$$rh'(\phi)V'(r)\phi'(r) + h(\phi) \left[-((z - D + 1)V'(r) + rV''(r)) \right] = 0. \quad (11)$$

Under these requirements(10), Eq.(11) becomes

$$V'(r) = \frac{Q}{h(\phi)} \left(\frac{l}{r}\right)^{D-1-z}, \quad (12)$$

in which Q is an arbitrary constant, and takes the role of the electric charge.

Dealing with the difference for components of Einstein field equations (5), one can find the identity

$$E^t_t - E^r_r = \frac{f(r)[(D-2)(1-z) + r^2\kappa\phi'(r)^2]}{l^2} = 0; \quad (13)$$

$$E^r_r + E^\theta_\theta = -\frac{(D-3)^2}{r^2} + 2\lambda + \frac{(z+D-3)(z+D-2)f(r)}{l^2} + \frac{r(3(z+D-2)-1)f'(r)}{2l^2} + \frac{r^2f''(r)}{2l^2} = 0. \quad (14)$$

Then, we obtain the solution for the scalar field $\phi(r)$ and $f(r)$ in generalized Einstein-Maxwell-Dilaton gravity from Eqs.(13) and (14)

$$\phi(r) = \phi_0 + \sqrt{\frac{(D-2)(z-1)}{\kappa}} \ln\left(\frac{r}{l}\right); \quad (15)$$

$$f(r) = 1 + \frac{kl^2(D-3)^2}{r^2(z+D-4)^2} + \frac{a}{r^{z+D-2}} + \frac{b}{r^{2(z+D-3)}}, \quad (16)$$

where a , b and ϕ_0 is an integration constant. Obviously, this solution is valid for $z \geq 1$.

By inserting the expression of the solutions $\phi(r)$, $V'(r)$ and $f(r)$ in the set of equations presented in the Einstein equation (5), as a consequence the nonminimal coupling function $h[\phi(r)]$ becomes

$$\begin{aligned}
h[\phi[r]] &= \left[Q^2 l^2 \kappa (z + D - 4) e^{-2\sqrt{\frac{(D-2)\kappa}{z-1}}(\phi-\phi_0)} \right] * \left[(z-1)(z+D-4)(z+D-2) \right. \\
&+ (D-2)b e^{-2(z+D-3)\sqrt{\frac{\kappa}{(D-2)(z-1)}}(\phi-\phi_0)} l^{-2(z+D-3)} (z+D-4)^2 \\
&\left. + k(D-2)(D-3)(z-1) e^{-2\sqrt{\frac{\kappa}{(D-2)(z-1)}}(\phi-\phi_0)} \right]^{-1}. \tag{17}
\end{aligned}$$

Suppose Maxwell equations accept trivial first integrals, the gauge potential is

$$\begin{aligned}
A(r) &= V_0 - \frac{(D-2)b}{Q\kappa l^{2(z+D)-5}} \left(\frac{l}{r}\right)^{z+D-4} + \frac{(z-1)}{Q\kappa l} \left(\frac{r}{l}\right)^{z+D-2} \\
&+ \frac{k(D-2)(D-3)(z-1)}{Q\kappa l(z+D-4)^2} \left(\frac{r}{l}\right)^{z+D-4}, \tag{18}
\end{aligned}$$

where V_0 is an integration constant. The remaining scalar field equation (4) are left for checking

$$\frac{r^2 \left(\frac{r}{l}\right)^{-2z} h'(\phi(r)) V'(r)^2}{2l^2} + \frac{r(rf'(r)\phi'(r) + f(r)((z+D-1)\phi'(r) + r\phi''(r)))}{l^2} = 0. \tag{19}$$

Altogether, in the present form, all solutions satisfy the whole set of equations of motion, and the metric function must satisfy the asymptotic condition

$$\lambda = -\frac{(z+D-3)(z+D-2)}{2l^2}. \tag{20}$$

III. QUASI-NORMAL MODES

It is assumed that the coupled charged massive scalar field in the background of a Lifshitz black hole satisfies the Klein-Gordon equation

$$D^\nu D_\nu \psi = m_s^2 \psi, \tag{21}$$

where $D^\nu = \nabla^\nu - iq_s A^\nu$ is the gauge covariant derivative and m_s is the mass of the scalar field ψ . Now we decompose ψ into the following standard form:

$$\psi(t, r, \text{angles}) = e^{-i\omega t} R(r) Y(\text{angles}), \tag{22}$$

where ω is the frequency and $Y(\text{angles})$ is the spherical harmonic function related to the angular coordinates. Since Y is the spherical harmonic function, it satisfies the following equation

$$\nabla_{\text{angles}}^2 Y(\theta, \phi) = -L(L+1)Y(\text{angles}), \tag{23}$$

where $L(L+1)$ is the constant of separation. In addition, the differential equation of the radial function in the D-dimensional Lifshitz-dilaton background (8) is

$$fR'' + \left(f' + \frac{(D+z-1)f}{r}\right)R' + \left(\frac{q_s A_t + \omega}{r^{z+1}}\right)^2 \frac{R}{f} - \left(m_s^2 + \frac{L(L+1)}{r^2}\right) \frac{R}{r^2} = 0. \tag{24}$$

Therefore, introducing a new radial function $R(r)$ as $R(r) = K(r) \times r^{1-\frac{D}{2}}$ and using a tortoise coordinate r_* as $dr_*/dr = [r^{z+1}f(r)]^{-1}$, the Eq. (24) can be transformed into an equation resembling the Schrödinger equation

$$\frac{d^2 K(r_*)}{dr_*^2} + [(\omega + q_s A_t)^2 - V(r)]K(r_*) = 0, \quad (25)$$

where the potential $V(r)$ is given by

$$V(r) = \left(\frac{D^2}{4} + \frac{Dz}{2} + 1 - D - z\right)f^2 r^{2z} + f r^{2z} \left(m_s^2 + \frac{L(L+1)}{r^2}\right) + f f' r^{2z+1} \left(\frac{D}{2} - 1\right). \quad (26)$$

To achieve a comprehensive understanding of the system's behavior, we need to conduct a numerical analysis. In this section, we will utilize the improved asymptotic iteration method (AIM) to analyze the behavior of QNMs numerically. We will begin by changing the variable $u = 1 - \frac{r_h}{r}$, and write Eq. (24) as

$$\begin{aligned} \frac{r_h^{z+1} f(u)}{(1-u)^{z-1}} R''(u) + \frac{r_h^{z+1}}{(1-u)^z} [(D+z-3)f(u) + (1-u)f'(u)] R'(u) + \frac{r_h^{1-z} l^{2z+2}}{f(u)(1-u)^{1-z}} \\ (q_s A_t(u) + \omega)^2 R(u) - \frac{r_h^{z+1}}{(1-u)^{z+1}} \left(m_s^2 + \frac{L(L+1)}{r_h^2} (1-u)^2\right) R(u) = 0. \end{aligned} \quad (27)$$

In order to propose an ansatz for Eq.(27), we are going to consider the behavior of the function $R(u)$ at horizon ($u = 0$), and boundary ($u = 1$). At horizon ($u = 0$), we have $f(0) \approx u f'(0)$ and $A_t(0) = 0$, thus Eq.(27) can be written as

$$R''(u) + \frac{R'(u)}{u} + \frac{R(u)}{r_h^{2z} u^2 f'^2} \omega^2 = 0. \quad (28)$$

The solution for this equation can be written as

$$R(u \rightarrow 0) \sim C_1 u^{-\xi} + C_2 u^\xi, \quad \xi = \frac{i\omega}{r_h^z f'(0)}. \quad (29)$$

Here we have imposed the ingoing boundary condition at the horizon ($u = 0$), and so we have required C_2 to vanish. At infinity, where ($u = 1$), Eq. (27), can be written as

$$R''(u) + \frac{(z+D-3)R'(u)}{1-u} - \frac{m_s^2 R(u)}{(1-u)^2} = 0. \quad (30)$$

The solution to this equation can be written as

$$R(u \rightarrow 1) \sim D_1 (1-u)^{\frac{1}{2}(z+D-2+\Pi)} + D_2 (1-u)^{\frac{1}{2}(z+D-2-\Pi)}, \quad (31)$$

where

$$\Pi = \sqrt{(z+D-2)^2 + 4m_s^2}. \quad (32)$$

In order to impose Dirichlet boundary condition $R(u \rightarrow 1) \rightarrow 0$, we can set $D_2 = 0$. Using the above solutions at horizon and boundary, the general ansatz for Eq. (27), can be written as

$$R(u) = u^{-\xi}(1-u)^{\frac{1}{2}(z+D-2+\Pi)}\chi(u). \quad (33)$$

Inserting Eq. (33) into (27), we obtain

$$\chi'' = \lambda_0(u)\chi' + s_0(u)\chi, \quad (34)$$

where the coefficient functions are given by

$$\lambda_0 = \frac{2i\omega}{r_h^z u f'(0)} - \frac{f'(u)}{f(u)} + \frac{\Pi + 1}{1 - u}. \quad (35)$$

Furthermore, s_0 is given by

$$\begin{aligned} s_0(u) = & \frac{r_h^{-2(z+1)}}{2(u-1)^2 u^2 f(u)^2 f'^2} \times [-2r_h^2 u^2 f'^2 (1-u)^{2z} (q_s A_t(u) + \omega)^2 \\ & + u f(u) f'(0) r_h^z (2u f'(0) r_h^z (m_s^2 r_h^2 + L(L+1)(u-1)^2) + r_h^2 (u-1) f'(u) \\ & \times (-u f'(0) r_h^z (\Pi + D + z - 2) + 2i(u-1)\omega) \\ & + 2r_h^2 f(u)^2 (i(u-1)\omega f'(0) r_h^z (u\Pi + 1) - m_s^2 u^2 f'^2 r_h^{2z} + (u-1)^2 \omega^2)]. \end{aligned} \quad (36)$$

Now we can employ the improved asymptotic iteration method (AIM) to numerically solve the Eq. (34). In the following, we set $l = 1$ and $L(L+1) = 2$, and analyze scalar perturbations and explore the impact of different model parameters on the real and imaginary components of the quasinormal frequencies related to Lifshitz black hole solutions.

IV. NUMERICAL RESULTS

In this section, we report our numerical results of the QNMs for the scalar field around Lifshitz black hole. We will consider the D-dimensional Lifshitz model under three different geometric properties ($k = 0, \pm 1$). The frequencies of the quasi-normal modes are divided into real and imaginary parts, which determine the energy of the scalar perturbations and the stability of the system under dynamical perturbations.

Let's first observe the imaginary part of the quasinormal frequency shown in Figure 1(a), $\omega_I < 0$ means the scalar field perturbations dissipate over time, indicating that the black hole system is approaching stability. When we fix other parameters related to black holes, we can draw conclusions by adjusting the mass-related parameter a , the absolute value of the imaginary part gradually increases with the increase of mass $|a|$. As we increase the charge-related parameter b from 0 in the

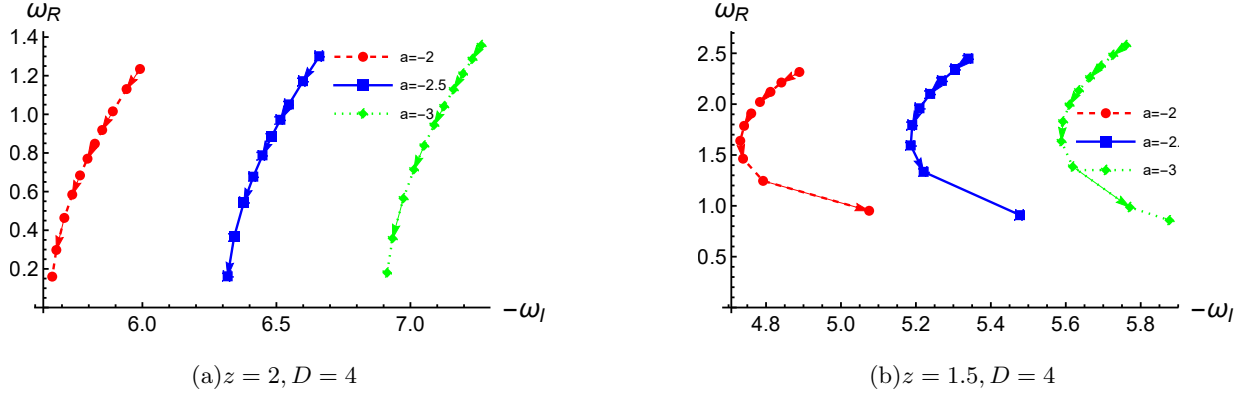


FIG. 1: The behaviors of real and imaginary parts of QNMs in the case with $k = 0$, $m_s = 0$, $q_s = 0$ for different a, b, z and D . The increase of the black holes charge b from 0 is shown with the arrows.

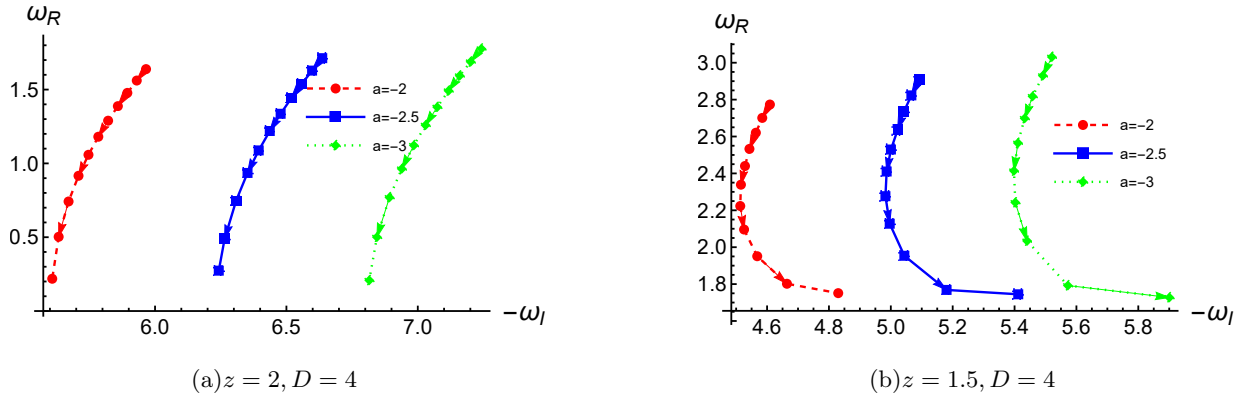


FIG. 2: The behaviors of real and imaginary parts of QNMs in the case with $k = 1$, $m_s = 0$, $q_s = 0$ for different a, b, z and D . The increase of the black holes charge b from 0 is shown with the arrows.

black hole background, $|\omega_I|$ gradually decreases, which indicates that scalar perturbations outside the black hole require a longer time to fully decay. From a holographic perspective, this suggests that the dual system requires a longer time to reach equilibrium. If we consider a smaller dynamical critical exponent z in Figure 1(b), the absolute value of the imaginary part begins to increase after reaching a minimum value. The increase of $|\omega_I|$ indicates that disturbances outside the black hole take a shorter time to dissipate. The situations under the geometric properties of $k = 1$ (Figure 2) and $k = -1$ (Figure 3) are similar to the trend observed in $k = 0$ (Figure 1). In Figures 4, 5 and 6, The quasinormal mode frequencies for $D = 5$ are presented, showing that only in Figure 6(a) does the imaginary part of the frequency exhibit a different trend, it initially decreases and then increases as b increases, in all other cases, the absolute value of the imaginary part of the frequency increases with the increase of b . This indicates that dimensions, critical dynamical exponents, and geometric properties all affect the quasi-normal modes, thereby influencing the decay time and

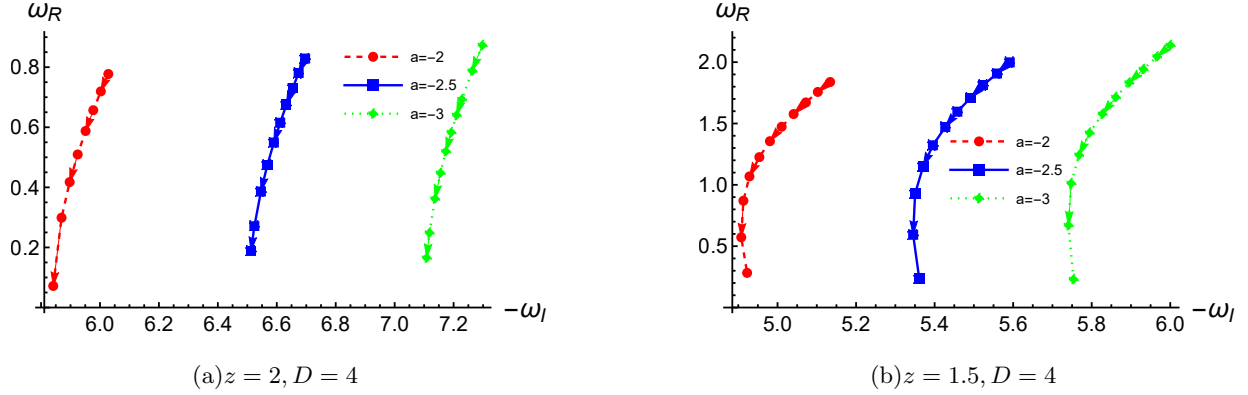


FIG. 3: The behaviors of real and imaginary parts of QNMs in the case with $k = -1$, $m_s = 0$, $q_s = 0$ for different a, b, z and D . The increase of the black holes charge b from 0 is shown with the arrows.

stability of black holes.

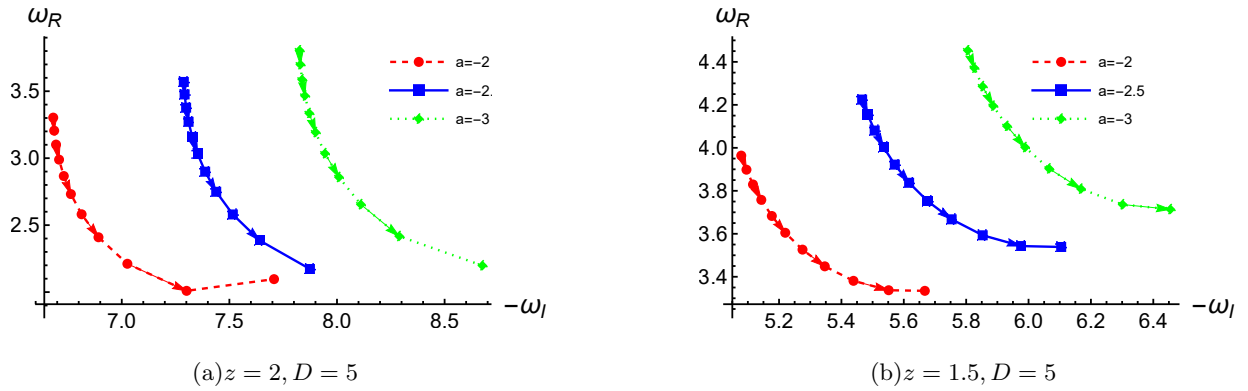


FIG. 4: The behaviors of real and imaginary parts of QNMs in the case with $k = 0$, $m_s = 0$, $q_s = 0$ for different a, b, z and D . The increase of the black holes charge b from 0 is shown with the arrows.

Now, let's turn our attention to the study of the real part of the frequency. By integrating the real part of the frequency from all the plots, we can observe that as the charge-related parameter b increases, the real part gradually decreases. This indicates that the energy of the scalar perturbation is gradually diminishing. When we select a larger black hole mass $|a|$, a smaller dynamic critical exponent z , greater curvature k , and a higher number of dimensions D , the maximum value of the real part of the frequency will increase.

In Figures 7, 8 and 9, the characteristics of the real and imaginary parts of the quasinormal mode frequencies, as they vary with the dynamic critical exponent z under different black hole masses, are presented. In the cases of $k = 0$ and $k = 1$, as the critical dynamical exponent z increases, the real part of the quasinormal mode frequencies first slightly increases to a maximum value and then

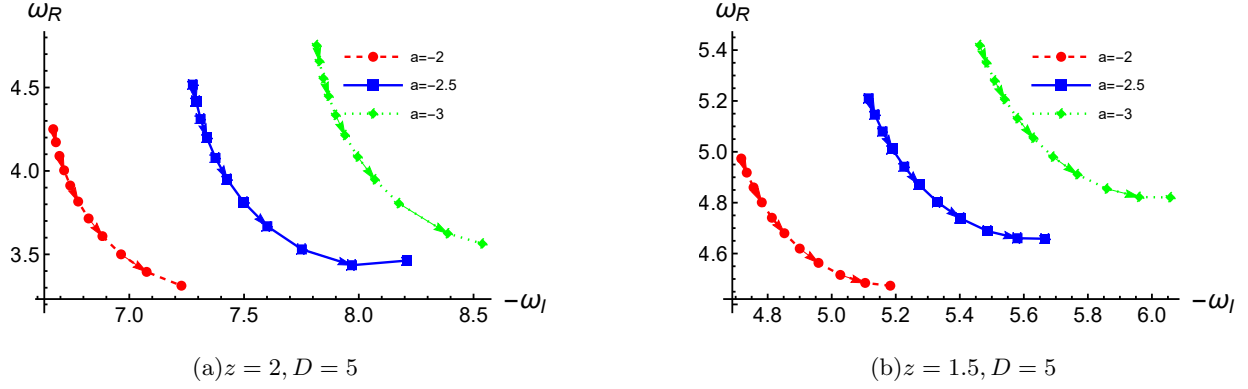


FIG. 5: The behaviors of real and imaginary parts of QNMs in the case with $k = 1$, $m_s = 0$, $q_s = 0$ for different a, b, z and D . The increase of the black holes charge b from 0 is shown with the arrows.

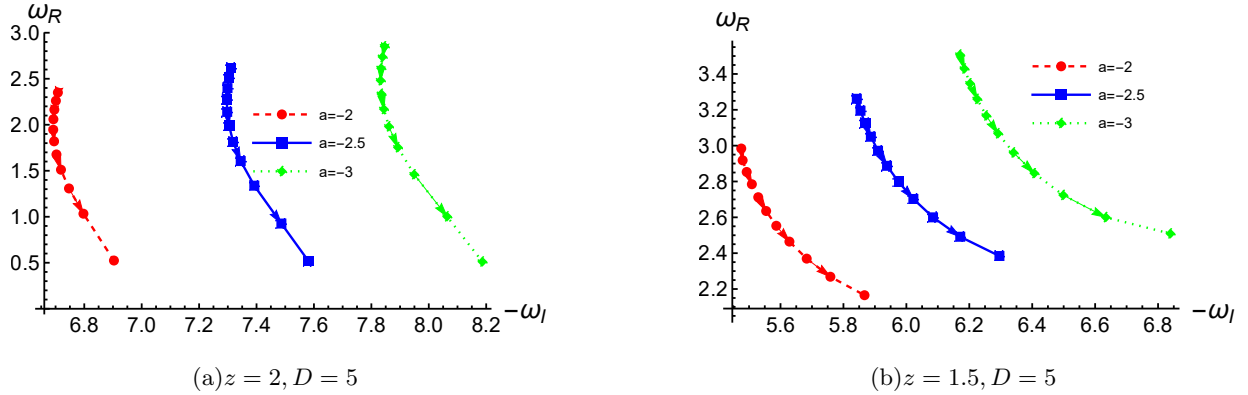


FIG. 6: The behaviors of real and imaginary parts of QNMs in the case with $k = -1$, $m_s = 0$, $q_s = 0$ for different a, b, z and D . The increase of the black holes charge b from 0 is shown with the arrows.

gradually decreases, while the absolute value of the imaginary part gradually increases. Unlike the previous two cases, in the case of $k = -1$, the imaginary part of the quasinormal mode frequencies directly decrease without an increasing trend.

V. CLOSING REMARKS

In this paper, we have constructed static asymptotically high-dimensional Lifshitz black hole solutions with a cosmological constant in the Einstein-Maxwell-Dilaton theory under three different horizon geometries. An important aspect of black hole physics is the study of the scattering resonances of incident waves by black holes. The QNMs of black holes can be used to calculate models in extra dimensions under a Lifshitz background. This paper calculates the quasinormal modes in the Einstein-Maxwell-Dilaton model with coupling between the Maxwell field and the

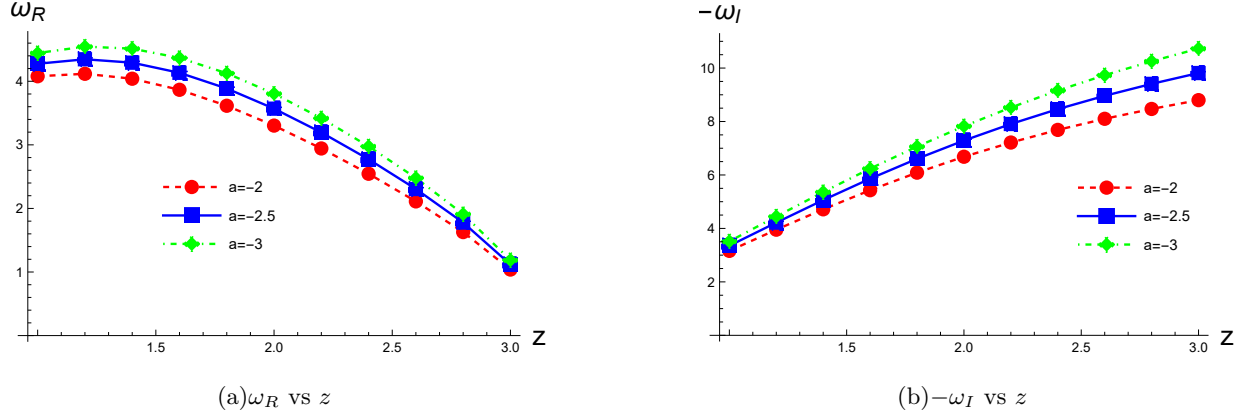


FIG. 7: The behaviors of real and imaginary parts of QNMs vs z for different a where $k = 0$, $D = 5$, $b = 0$, $m_s = 0$, $q_s = 0$.

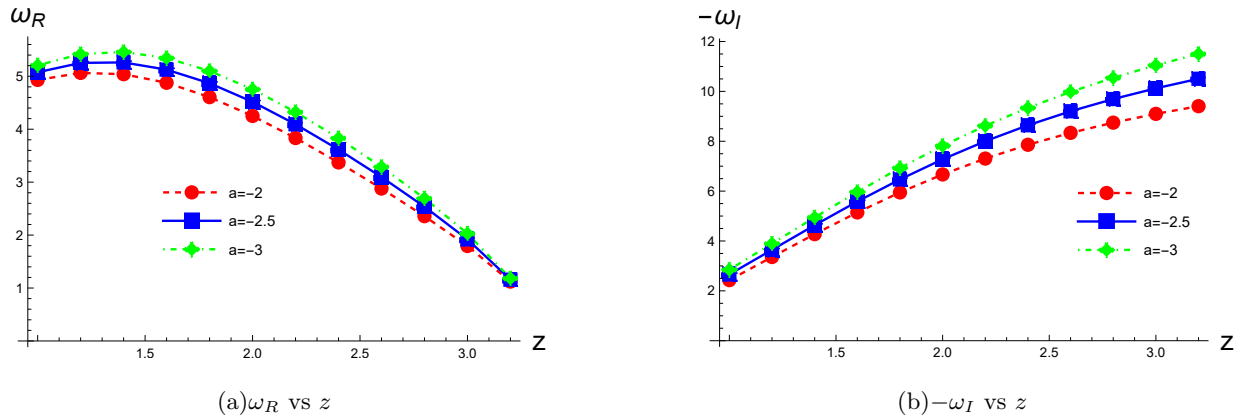


FIG. 8: The behaviors of real and imaginary parts of QNMs vs z for different a where $k = 1$, $D = 5$, $b = 0$, $m_s = 0$, $q_s = 0$.

scalar field.

Specifically, we will employ the improved asymptotic iteration method (AIM) to numerically compute the scalar perturbations of the EMD model. We will investigate the effects of different black hole parameters on the real and imaginary parts of the QNMs. In the case of $z = 2$, $D = 4$, the absolute value of the imaginary part of the quasinormal mode frequency and the real part decrease as the charge-related quantity b increases. For $z = 1.5$, $D = 4$, the absolute value of the imaginary part of the quasinormal mode frequency first reaches a maximum before decreasing. In the case of $D = 5$, the absolute value of the imaginary part of the quasinormal mode frequency increases with b , while the real part gradually decreases. Notably, only when $k = -1$ does the absolute value of the imaginary part of the quasinormal mode frequency experience a brief decrease before increasing again. A larger black hole mass $|a|$, a smaller dynamic critical exponent z , a larger curvature k ,

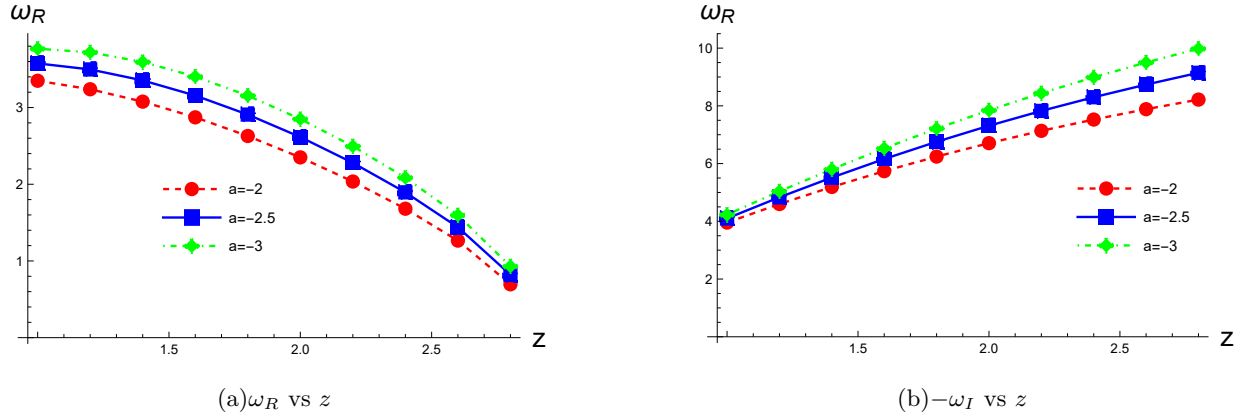


FIG. 9: The behaviors of real and imaginary parts of QNMs vs z for different a where $k = -1$, $D = 5$, $b = 0$, $m_s = 0$, $q_s = 0$.

and a higher dimension D will result in an increase in the maximum real part of the frequency. This trend can be attributed to the interplay between these parameters, which affects the stability and oscillatory behavior of the black hole's QNMs. Specifically, larger mass and curvature can enhance the gravitational effects, while a lower dynamic critical exponent and higher dimensions may influence the frequency characteristics, leading to an overall increase in the maximum value of the real part of the frequency. The increase or decrease in the absolute value of the imaginary part of the quasinormal mode frequency symbolizes that the decay time of the perturbation becomes shorter or longer with the increase of charge; the decrease in the real part of the QNMs indicates that the energy of the black hole is gradually diminishing.

Acknowledgments

D. C. Z is supported by the Natural Science Foundation of China (NSFC) (Grant No.12365009) and Natural Science Foundation of Jiangxi Province (Grant No. 20232BAB201039). M. Z. is supported by Natural Science Basic Research Program of Shaanxi (Program No.2023-JC-QN-0053).

-
- [1] R. Ruffini and J. A. Wheeler, "Introducing the black hole," *Phys. Today* **24** (1971) no.1, 30 doi:10.1063/1.3022513
- [2] J. D. Bekenstein, "Nonexistence of baryon number for static black holes," *Phys. Rev. D* **5** (1972), 1239-1246 doi:10.1103/PhysRevD.5.1239

- [3] M. J. Perry, “Black Holes Are Colored,” *Phys. Lett. B* **71** (1977), 234-236 doi:10.1016/0370-2693(77)90786-9
- [4] D. V. Galtsov and A. A. Ershov, “Nonabelian Baldness of Colored Black Holes,” *Phys. Lett. A* **138** (1989), 160-164 doi:10.1016/0375-9601(89)90019-4
- [5] P. Kanti, N. E. Mavromatos, J. Rizos, K. Tamvakis and E. Winstanley, “Dilatonic black holes in higher curvature string gravity,” *Phys. Rev. D* **54** (1996), 5049-5058 doi:10.1103/PhysRevD.54.5049 [arXiv:hep-th/9511071 [hep-th]].
- [6] H. Luckock and I. Moss, “BLACK HOLES HAVE SKYRMION HAIR,” *Phys. Lett. B* **176** (1986), 341-345 doi:10.1016/0370-2693(86)90175-9
- [7] C. A. R. Herdeiro and E. Radu, *Int. J. Mod. Phys. D* **24** (2015) no.09, 1542014 doi:10.1142/S0218271815420146 [arXiv:1504.08209 [gr-qc]].
- [8] T. Harada, *Phys. Rev. D* **57** (1998), 4802-4811 doi:10.1103/PhysRevD.57.4802 [arXiv:gr-qc/9801049 [gr-qc]].
- [9] T. Damour and G. Esposito-Farese, *Phys. Rev. D* **54** (1996), 1474-1491 doi:10.1103/PhysRevD.54.1474 [arXiv:gr-qc/9602056 [gr-qc]].
- [10] C. A. R. Herdeiro, E. Radu, N. Sanchis-Gual and J. A. Font, “Spontaneous Scalarization of Charged Black Holes,” *Phys. Rev. Lett.* **121** (2018) no.10, 101102 doi:10.1103/PhysRevLett.121.101102 [arXiv:1806.05190 [gr-qc]].
- [11] J. M. Maldacena, “The Large N limit of superconformal field theories and supergravity,” *Adv. Theor. Math. Phys.* **2** (1998), 231-252 doi:10.4310/ATMP.1998.v2.n2.a1 [arXiv:hep-th/9711200 [hep-th]].
- [12] O. Lunin and S. D. Mathur, “AdS / CFT duality and the black hole information paradox,” *Nucl. Phys. B* **623** (2002), 342-394 doi:10.1016/S0550-3213(01)00620-4 [arXiv:hep-th/0109154 [hep-th]].
- [13] A. Herrera-Aguilar, D. F. Higueta-Borja and J. A. Méndez-Zavaleta, “Scalarization-like mechanism through spacetime anisotropic scaling symmetry,” *Phys. Rev. D* **103** (2021) no.12, 124025 doi:10.1103/PhysRevD.103.124025 [arXiv:2012.13412 [hep-th]].
- [14] D. C. Moreira, A. S. Lemos and F. A. Brito, “Charged Lifshitz black holes from general covariance breaking,” *Class. Quant. Grav.* **41** (2024) no.4, 045004 doi:10.1088/1361-6382/ad1d47 [arXiv:2307.07305 [hep-th]].
- [15] I. Andrade, M. A. Marques, R. Menezes and D. C. Moreira, “Spatially localized scalar structures on hyperscaling violating geometries,” [arXiv:2401.14082 [hep-th]].
- [16] S. Kachru, X. Liu and M. Mulligan, “Gravity duals of Lifshitz-like fixed points,” *Phys. Rev. D* **78** (2008), 106005 doi:10.1103/PhysRevD.78.106005 [arXiv:0808.1725 [hep-th]].
- [17] R. A. Konoplya and A. Zhidenko, *Rev. Mod. Phys.* **83** (2011), 793-836 doi:10.1103/RevModPhys.83.793 [arXiv:1102.4014 [gr-qc]].
- [18] K. D. Kokkotas and B. G. Schmidt, *Living Rev. Rel.* **2** (1999), 2 doi:10.12942/lrr-1999-2 [arXiv:gr-qc/9909058 [gr-qc]].
- [19] B. Wang, *Braz. J. Phys.* **35** (2005), 1029-1037 doi:10.1590/S0103-97332005000700002 [arXiv:gr-

- qc/0511133 [gr-qc].
- [20] E. Berti, V. Cardoso, J. A. Gonzalez and U. Sperhake, Phys. Rev. D **75** (2007), 124017 doi:10.1103/PhysRevD.75.124017 [arXiv:gr-qc/0701086 [gr-qc]].
- [21] S. Chakraborty, K. Chakravarti, S. Bose and S. SenGupta, Phys. Rev. D **97** (2018) no.10, 104053 doi:10.1103/PhysRevD.97.104053 [arXiv:1710.05188 [gr-qc]].
- [22] S. Aneesh, S. Bose and S. Kar, Phys. Rev. D **97** (2018) no.12, 124004 doi:10.1103/PhysRevD.97.124004 [arXiv:1803.10204 [gr-qc]].
- [23] L. Visinelli, N. Bolis and S. Vagnozzi, Phys. Rev. D **97** (2018) no.6, 064039 doi:10.1103/PhysRevD.97.064039 [arXiv:1711.06628 [gr-qc]].
- [24] E. Berti, V. Cardoso and C. M. Will, Phys. Rev. D **73** (2006), 064030 doi:10.1103/PhysRevD.73.064030 [arXiv:gr-qc/0512160 [gr-qc]].
- [25] M. Isi, M. Giesler, W. M. Farr, M. A. Scheel and S. A. Teukolsky, Phys. Rev. Lett. **123** (2019) no.11, 111102 doi:10.1103/PhysRevLett.123.111102 [arXiv:1905.00869 [gr-qc]].
- [26] V. Cardoso and P. Pani, Living Rev. Rel. **22** (2019) no.1, 4 doi:10.1007/s41114-019-0020-4 [arXiv:1904.05363 [gr-qc]].